https://doi.org/10.5194/egusphere-2026-3716
Preprint. Discussion started: 27 July 2026


# Supercooled nitrate solution on ice at 232 K: Enhanced HONO yields

Yanisha Manoharan, Zoë M. Golay*, Jérôme P. Gabathuler, Anthony Boucly, Luca Artiglia, Markus Ammann, Thorsten Bartels-Rausch

PSI Center for Energy and Environmental Sciences, Paul Scherrer Institute PSI, Villigen, Switzerland
*Now at Department of Chemistry, University of British Columbia, Vancouver V6T1Z1, BC, Canada

*Correspondence*: Thorsten Bartels-Rausch (thorsten.bartels-rausch@psi.ch)

**Abstract.** Snowpack nitrate photolysis is a major source of nitrogen oxides and nitrous acid that control atmospheric oxidants in polar environments. It remains unclear at what temperature nitrate salts crystalize in snow and how this impacts the photolysis product yields. Here we show, using near-edge X-ray absorption fine structure (NEXAFS) spectroscopy, that sodium nitrate does not precipitate at temperatures down to 23 K below the eutectic temperature at ice surfaces, but does so in absence of ice. This indicates that strong interfacial supercooling or liquid-like solvation persists. Complementary snow photolysis experiments demonstrate that such liquid-like nitrate shows a higher HONO to $NO_2$ emission ratio than precipitated nitrate, which is consistent with the enhanced role of secondary chemistry in the aqueous phase. These findings show that supercooled nitrate might be present over wide ranges of Arctic, Antarctic, and upper tropospheric temperatures with a significant impact on the HONO and $NO_2$ fluxes and thus the composition and chemistry in the air above snow or in contact with ice clouds.

## 1 Introduction

Nitrate is one of the most abundant nitrogen species deposited from the atmosphere to snow and ice (Frey et al., 2009). In Polar regions, 75 % - 100 % of deposited nitrogen species are nitrates with typical snowpack concentrations on the order of 5 µM - 10 µM (Blaszczak-Boxe and Saiz-Lopez, 2018). Photolysis of nitrate in snow and ice is a major source of reactive nitrogen oxides ($NO_x$ = NO and $NO_2$) and nitrous acid (HONO), which affects the hydroxyl radical budget and ozone production in the upper troposphere and snow-covered remote and polar regions (Grannas et al., 2007). Recent field studies in Antarctica show that snowpack emissions from nitrate photolysis drive summertime HONO levels, exceeding gas-phase sources by an order of magnitude (Bond et al., 2023) and controlling HONO levels frequently on short time scales (Cheng et al., 2025). Improved understanding of the underlying multiphase chemistry remains a key topic in atmospheric research (Gen et al., 2022). Laboratory studies have systematically characterized nitrate photochemical reactivity in snow, ice, and water. HONO and $NO_2$ are formed via two nitrate photolysis channels in aqueous solution and in brine (Eqs. 1 and 2).

$$NO_3^- + h\nu\ (UVB)(+H^+) \rightarrow NO_2 + OH \text{ (Channel 1)} \quad \text{(Eq. 1)}$$

$$NO_3^- + h\nu\ (UVB) \rightarrow NO_2^- + O(^3P) \text{ (Channel 2)} \quad \text{(Eq. 2)}$$

https://doi.org/10.5194/egusphere-2026-3716
Preprint. Discussion started: 27 July 2026


In aqueous solution at room temperature, the quantum yields for Channel 1 and Channel 2 were recently found to be comparable at 313 nm, emphasizing that nitrite production can be a major pathway in nitrate photolysis (Benedict et al., 2017). In liquid-like regions (LLR) of ice, Benedict and Anastasio (2017) showed that these quantum yields follow a single Arrhenius relationship continuous from 25 °C to -30 °C, with Channel 2 becoming increasingly dominant at lower temperatures. Crucially, no discontinuity was observed in the quantum yields in those LLR experiments. Chan et al. (2025) recently provided an explanation for the temperature dependence through first-principles molecular dynamics simulations: after excitation to the triplet state, nitrate forms a metastable solvation cage with surrounding water molecules, and the branching between the two channels is controlled by hydrogen-bond rearrangement within that cage. Channel 1 requires a more extensive H-bond reorganization and therefore becomes thermally less accessible at lower temperatures. This framework identifies the local solvation environment as the determinant of photochemical channel branching. McFall et al. (2018a) showed a quantitative comparison across ice reservoirs: While LLR quantum yields match aqueous values at the same temperature, the air–ice interface shows a 3.7-fold enhancement, with this enhancement factor essentially temperature-independent over the -5 °C to -25 °C range. Hullar et al. (2023) confirmed this surface enhancement using nature-identical snow with environmentally relevant nitrate coverages, finding a 6.4-fold enhancement relative to aqueous solution. Computational work has addressed how the nitrate solvation environment defines its photochemical reactivity: Berrens et al. (2023) showed through first-principles calculations that the local hydrogen-bonding structure at the air–ice interface modifies the UV–visible absorption cross-section of nitrate.

Here, we study the solvation environment of nitrate at the air-ice interface. Phase changes and precipitation of solutes have a direct impact on the photochemical reactivity in ice and snow (Bartels-Rausch et al., 2014; Grannas et al., 2007; Kahan et al., 2014a). For nitrate in aerosol particles, changes in phase state have been shown to exert a strong impact on HONO release, as recently demonstrated in laboratory and field studies study (Andersen et al., 2023; Shi et al., 2021). Morenz and Donaldson (2017) have shown that at the eutectic temperature, 255 K for $NaNO_3$ (Van der Ham et al., 1998), aqueous nitrate solution, and precipitated $NaNO_3$ coexist and this raises questions regarding the phase state of nitrate at temperatures below this point. We have recently shown significant supercooling of NaCl solutions at ice surfaces (Bartels-Rausch et al., 2021), and the extent to which this happens to $NaNO_3$ remains open.

To study changes to the local hydrogen-bonding of $NaNO_3$ at the ice surface, we use near edge X-ray absorption fine structure (NEXAFS) spectroscopy. NEXAFS spectroscopy provides element specificity, allowing the characterization of the local solvation environment of selected solutes (Bartels-Rausch et al., 2021; Kong et al., 2020; Křepelová et al., 2010a). When detecting electrons, as in this work, probing depths as low as a few nanometers can be achieved, making this method inherently sensitive to interfacial environments (Ammann et al., 2018). Previous NEXAFS studies of salt-ice mixtures have revealed details on phase changes and distribution of brine or salt on ice. Křepelová et al. (2010a) probed oxygen in NaCl ice mixtures

https://doi.org/10.5194/egusphere-2026-3716
Preprint. Discussion started: 27 July 2026


(O K-edge NEXAFS). While these spectra were dominated by the ice signal, they allowed estimates of the liquid fraction and the solvation environment of NaCl. Subsequent Cl K-edge NEXAFS measurements provided direct evidence for interfacial supercooling of sodium chloride (Bartels-Rausch et al., 2021). Building on these works, we combine Na K-edge NEXAFS and N K-edge NEXAFS spectroscopy with controlled cooling and warming trajectories to probe the phase state and local solvation environment of $NaNO_3$ at the air–ice interface. N K-edge NEXAFS is particularly sensitive to the solvation environment of nitrate, showing systematic differences between crystalline $NO_3^-$ (Preobrajenski et al., 2002) and aqueous $NO_3^-$ (Smith et al., 2015). For sodium, changes in the local environment induced by water adsorption were revealed by means of Na K-edge NEXAFS spectra (Kong et al., 2020).

Solutes can also substantially modify the interfacial hydrogen bonding network in absence of phase changes (Ammann et al., 2018) and NEXAFS spectra probing the O K-edge of water molecules at the interface in presence of nitric acid ($HNO_3$) have demonstrated such adsorbate induced liquid-like environments (Křepelová et al., 2010b). Molecular dynamics simulations (Chan et al., 2025; Yasuda et al., 2024) predict that ions at the ice interface disrupt the local hydrogen-bonding network. Computational work further shows that these disordered interfacial environments can persist well below the eutectic temperature. Recent simulations of ice growth from saline solutions show ion rejection to the interface (Armstrong et al., 2025). The finding of Benedict and Anastasio (2017) that LLR quantum yields show no change at the $NaNO_3$ eutectic is consistent with nitrate remaining solvated below that temperature. Yet, it leaves unanswered if supercooled nitrate solutions persist at the ice surface and what happens to the reactivity when nitrate actually crystallizes, a condition that can arise in the absence of ice or when the supercooling limit is exceeded. Consistent with earlier experimental observations of liquid-like features induced by adsorbed acidic trace gases (Bartels-Rausch et al., 2014; Kong et al., 2017; Křepelová et al., 2010b), our measurements do not aim to distinguish between a quasi-liquid layer and interfacial brine. Rather, we focus on the local solvation environment of nitrate at the ice interface, as both processes provide aqueous-like hydration environments that are relevant for interfacial reactivity (Bartels-Rausch et al., 2025; Ruiz-Lopez et al., 2020). In addition, complementary snow photolysis experiments are used to assess how nitrate phase state influences the relative photolysis emissions of $NO_2$ and HONO.

The solvation state of $NaNO_3$ at ice surfaces below the eutectic temperature, and its consequences for photolysis product branching, remain open questions that prior bulk-sensitive and ice-interface studies have not directly resolved. In this work we address them by combining the Na K-edge and N K-edge NEXAFS measurements with the snow photolysis experiments described above, comparing samples in the presence and absence of ice across a range of temperatures spanning the eutectic.

https://doi.org/10.5194/egusphere-2026-3716
Preprint. Discussion started: 27 July 2026


## 2 Experimental Section

The near ambient pressure X-ray photoelectron spectroscopy (XPS) experiments were carried out at the In-Situ Spectroscopy (ISS) beamline of the Swiss Light Source (SLS) at the Paul Scherrer Institute (PSI) using the solid-gas interface endstation (Orlando et al., 2016). The starting point of each experiment was the anhydrous sodium nitrate salt on a gold-coated sample holder. Sodium nitrate powder (Sigma Aldrich, ≥ 99.9%) was ground in a mortar and mixed with a water-alcohol mixture in an ultrasonic bath to produce a saturated solution, of which 0.1 µl was drop-cast with a micro-syringe onto the sample holder at 60 °C. Methanol (Sigma Aldrich, HPLC grade ACS ISO UV-VIS K.F.) or a mixture of water (Alfa Aesar, ultrapure, HPLC grade) and ethanol (VWR Chemicals, absolute, HPLC grade) with a ratio of 1:3 was used as a solvent. The drops were dried with a heat gun, and the dried salt on the sample holder was mounted in a temperature and humidity controlled experimental cell for experiments described below. The experimental cell holds the temperature controlled sample, gas inlets, the entrance orifice to the electron analyzer (cone), and a window to transmit the X-ray from the beamline to the sample (Orlando et al., 2016). The salt sample was left under UHV for a minimum of 15 minutes prior to the start of the experiment to evaporate the remaining solvent. NEXAFS spectra of the anhydrous $NaNO_3$ solid were aquired at less than 5.0% relative humidity and at a temperature of either 293 K or 298 K. This low amount of water was added to the gas-phase to reduce charging of the sample during the X-ray excited electron spectroscopy measurements. The water (Alfa Aesar, ultrapure, HPLC grade) was degassed prior to use by five freeze-pump-thaw cycles.

Experiments followed controlled paths across the $NaNO_3$–$H_2O$ phase diagram to either include or exclude ice (Fig. 1). Phase change from crystalline salt to an aqueous solution of $NaNO_3$ with ice (brine) was caused by first increasing the dosing water vapor pressure to typically 1.9 mbar at 260 K crossing the solubility line (Figure 1). Complete deliquescence of the salt was inspected visually with an endoscope. Then the partial pressure of water was further increased to typically 2.1mbar to cross the liquidus line (Fig. 1) and form an ice-brine mixture. Finally, temperature was lowered below the eutectic while keeping the ice in equilibrium by following the liquidus line extrapolated to temperatures below the eutectic point and back (Fig. 1). This was achieved by adjusting the dosing water vapor pressure and the sample temperature simultaneously. A calibration measurement was performed, where the pressure in the experimental cell resulting solely from water vapor dosing was measured for each temperature of the dosing reservoir. This calibration procedure was required, because once ice formed, the water vapor pressure in the experimental cell was a sole function of the temperature. The vapor pressure of ice determines the cell water pressure and not the flux into the cell. (Fig. 1, open squares and diamonds). If the dosing vapor pressure of water was higher than the equilibrium vapor pressure of ice at the specific temperature, the ice grew. In absence of ice, the dosing flux of water at the given pump velocity determines the partial pressure and any region in the phase diagram can be reached (Fig. 1, open triangles). Somewhat in contrast, the composition of the brine, thus its water activity, is always consistent with the water vapor pressure in the cell, independent of whether the latter is determined by the presence of ice or by the water vapor pressure at a given temperature in absence of ice. Overall, water partial pressures were between 0.1 and 2.5 mbar and sample temperatures were between 264 K and 232 K, depending on the experiment.

https://doi.org/10.5194/egusphere-2026-3716
Preprint. Discussion started: 27 July 2026


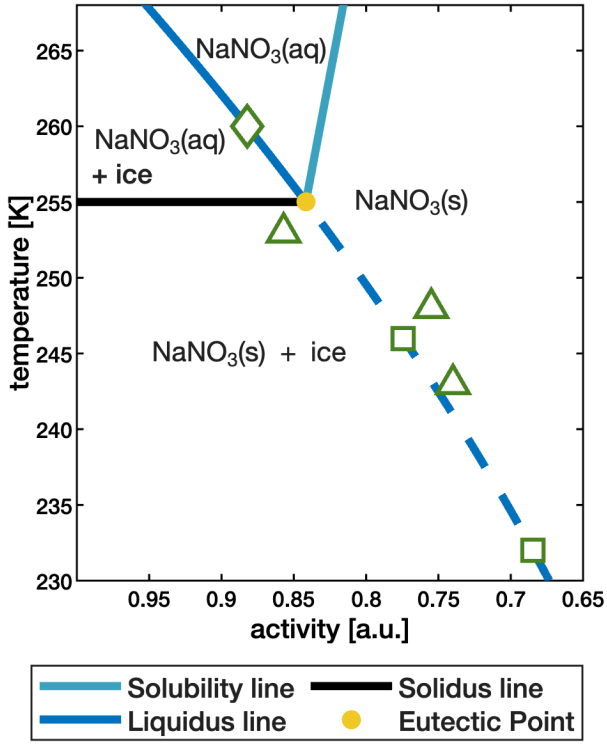


**Figure 1: Binary phase diagram of sodium nitrate and water, with the activity of water on the x-axis and temperature on the y-axis. The water activity is a measure of the relative humidity with an activity of 1 corresponding to 100% RH. The solubility line (deliquescence curve) separates the solid salt from the aqueous phase of $NaNO_3$ (Tang and Munkelwitz, 1993) and the liquidus line (freezing point curve) separates the ice phase and the aqueous solution from the aqueous phase (Bridgeman and Aldrich, 1964; Marti and Mauersberger, 1993). The solidus line indicates the warmest temperature where ice and crystalline salt may coexist. Between the liquidus line and deliquescence curve, $NaNO_3$ is present in the form of an aqueous phase and in the absence of the solid form of the salt. Note that the liquidus line was extended to temperatures below the eutectic (dashed blue line) following the parameterization of saturation vapor pressure with respect to ice (Koop and Zobrist, 2009; Murphy and Koop, 2005). Also shown are the temperature and water activity settings of the data discussed in this work (open diamond, Fig. 2; open square, Fig. 3a; open triangle, Fig. 3b)**

The Na K-edge NEXAFS spectra were acquired with a pass energy of 100 eV or 50 eV, dwell time of 0.2 s, and monochromator entrance and exit slit set to 1.0. For the excitation in the Na K-edge region, the photon energy range was set to 1068 eV to 1110 eV in 0.25 eV steps. The Na K-edge spectra were recorded in sweep mode with minor variations in the kinetic energy window of the Auger-Meitner electrons of 947 eV to 972 eV, 947 eV to 960 eV, or from 967 eV to 992 eV. These kinetic energy regions were free from any other photoemission peaks. Integrating over the absorption feature at the kinetic energy of 985 eV (Auger-Meitner peak) or over the feature at 960 eV (inelastically scattered Auger-Meitner electrons) was observed not to make any difference in the shape of the absorption spectrum. The only difference was the overall intensity, which was lower when integrated at around 960 eV than at around 985 eV. The photon energy for the nitrogen K-edge region was selected to range from 385 eV to 398 eV in 0.5 eV steps, from 398 eV to 415 eV in 0.25 eV steps, and from 415 eV to 430 eV in 0.5 eV steps. The N K-edge spectra were recorded in sweep mode at a kinetic energy of the Auger-Meitner electrons

https://doi.org/10.5194/egusphere-2026-3716
Preprint. Discussion started: 27 July 2026


ranging from 300 to 350 eV. NEXAFS data were normalized to the photon flux, which was measured at the sample position with a Si PIPS photodiode (Bartels-Rausch et al., 2023). The beamline monochromator was energy calibrated using the N K-edge NEXAFS spectra of gas-phase $N_2$ based on the absorption feature at 401 eV coming from the $1s \rightarrow 1\pi_g^*$ transition (Chen et al., 1989). A constant offset in X-ray photon energy of 2.0 ± 0.2 eV was determined for all experiments. If multiple NEXAFS spectra were acquired at the same conditions, they were averaged resulting in a higher signal to noise ratio. Further processing was done by subtracting the mean pre-edge intensity as background and normalizing to the mean intensity in the range of 1071 eV and 1100 eV.

To assess the impact of Na nitrate precipitation on nitrate photolysis, flow tube studies with packed nitrate-doped, artificial snow were performed in analogy to earlier studies (Edebeli et al., 2020). Snow was prepared from solutions, Na nitrate (Sigma Aldrich, ≥ 99.9%) in ultrapure deionized water with a concentration of 25 µM and a pH of 3.0. The solution was decanted into a spray bottle and dispersed as fine droplets over a liquid nitrogen bath similar to earlier studies (Bartels-Rausch et al., 2004; Edebeli et al., 2020; Morenz et al., 2016; Wren et al., 2013). The droplets froze and sank to the bottom of the bath. The liquid nitrogen was removed, and the snow batch was stored at -30°C for at least 48 h, leading to recrystallization of the ice grains. The snow was then passed through a metal sieve to size-segregate the crystals, and the 500-600 µm sample size was selected for experiments. Snow grains were scooped into a quartz tube (16 mm diameter) which was plugged at both ends with glass wool. Once in the quartz tube, snow samples were approximately 4-7 cm in length, with a density of ~400-500 kg $m^{-3}$. The quartz tube was then connected to a flow system made of PFA tubes, inserted into a larger double-walled temperature-controlled quartz jacket surrounded by 7 UVB lamps (Ushio UV-B Midrange 159-00-820913506), or a combination of 3 UVA (Isolde, Cleo 61205240) and 4 UVB (Ushio UV-B Midrange 159-00-820913506), to maintain a constant cold temperature during radiation. A humidified flow of 125 mL/min $N_2$ and $O_2$ (80% and 20%) was passed through the snow. Upon leaving the sample, the gas-flow was diluted with 1500 mL/min $N_2$. Because of the high flow demands of the instruments, sample flow was diverted between one of two pathways to maintain measurable gas concentrations. The first pathway led to a HONO detector, an Iterative Cavity Differential optical absorption spectrometer (ICAD), for HONO quantification. The second pathway led to an $NO_2$ ICAD and a Teledyne NOx analyzer to detect gaseous $NO_2$ and NO. Irradiance at the sample position was measured using a spectroradiometer (Jeti, Specbos 1211) and a 90° remote diffusor (Jeti, ACC019UV).

## 3 Results and Discussion

### 3.1 Characterization of solid $NaNO_3$ salt and brine by NEXAFS

Figure 2 displays the Na K-edge NEXAFS spectrum of $NaNO_3$ salt and of an ice-$NaNO_3$ brine mixture at 260 K, that is above the eutectic temperature. Strong absorption features were detected at 1079 – 1081 eV and 1084 – 1085 eV in the salt sample which are attributed to the excitation of core electrons to the unoccupied orbitals in sodium (De Wispelaere et al., 2004; Murata et al., 1989a; Prado and Flank, 2005). The aqueous $NaNO_3$ Na K-edge NEXAFS spectrum is characterized by a shoulder at

https://doi.org/10.5194/egusphere-2026-3716
Preprint. Discussion started: 27 July 2026


1079 eV and an intense feature between 1083 – 1084 eV. The distinct absorption features of crystalline and aqueous $NaNO_3$ provide a clear basis for identifying aqueous $NaNO_3$ below the eutectic. The Na K-edge NEXAFS spectrum of $NaNO_3$ salt shows the typical shape also found for sodium halides and carbonates, and agrees well with reference spectra of sodium nitrate (Murata et al., 1989b; Rekhtina et al., 2023; Yoshimura et al., 2017). Published $NaNO_3$ Na K-edge NEXAFS spectra show fluctuations of the relative intensities of the two features, that Rekhtina et al. (2023) assigned to instrumental artefacts and the orientation of crystal grains relative to the polarization of the X-ray. To address instrumental artefacts in our experiments, we performed a test with extended measurement time, thereby increasing the X-ray dose and the associated beam-induced alterations of the sample (Aduru et al., 1986). This extended X-ray exposure resulted in one Na K-edge NEXAFS spectrum dominated by one peak at 1080 eV only. A second peak at 1084 – 1085 eV was absent, confirming the X-ray induced modifications of the sample (SI). Despite this, the peak at 1080 eV can be used to evaluate the presence of the solid as there was consistent shape and intensity for all solid $NaNO_3$ samples measured here independent of measurement settings.

Figure 2 also shows the Na K-edge NEXAFS spectra of aqueous $NaNO_3$ with the typical shape with a main feature at 1083 eV and a minor feature at 1079 eV known for sodium halides and sodium acetate (Aziz et al., 2006; Galib et al., 2017; Kong et al., 2020). The similarity between NaCl, $NaNO_3$ and sodium acetate might be due to the same local environment of water molecules, surrounding the sodium ion upon dissolution and solvation, independent of the counter ions. NEXAFS is sensitive only to the first hydration shell of the probed ion, particularly for a singly charged ion like the sodium cation (Ammann et al., 2018; Gopakumar et al., 2022). Note that the spectrum of the aqueous solution in an average of spectra acquired at different sample spots and at different temperatures between 2 K and 8 K above the eutectic and thus at different concentrations of $NaNO_3$ in the aqueous phase.

https://doi.org/10.5194/egusphere-2026-3716
Preprint. Discussion started: 27 July 2026


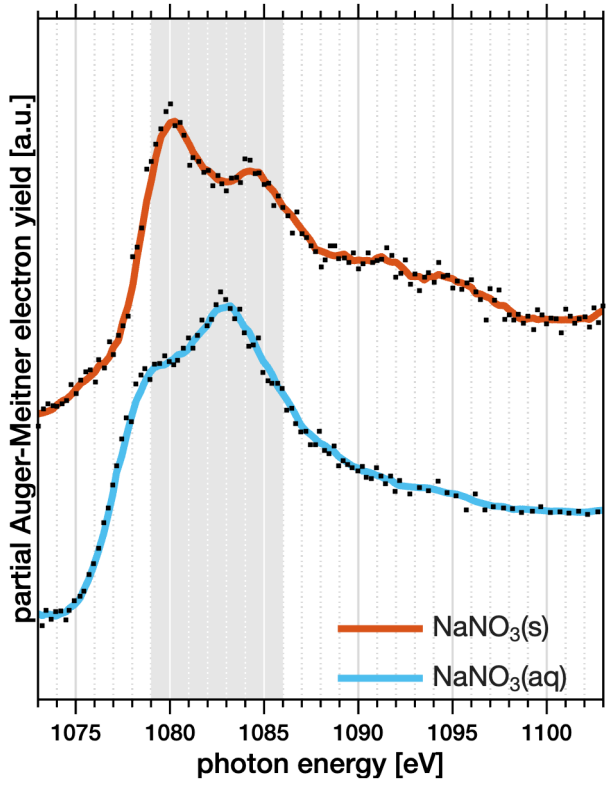


**Figure 2: Na K-edge NEXAFS spectra probing crystalline (red line) and aqueous sodium nitrate embedded in ice at 260 K (light blue line) with the partial Auger-Meitner electron yield in arbitrary units on the y-axis, and the photon energy in eV on the x-axis. Lines are moving averages and black dots are the data.**

### 3.2 Characterization of $NaNO_3$ below eutectic

Next, the temperature region below the eutectic was probed with the goal of investigating the local environment by identifying the crystalline and aqueous reference spectral features as seen above the eutectic temperature. Figure 3 shows Na K-edge NEXAFS spectra after cooling a sample from 257 K below the eutectic temperature of 255 K. The NEXAFS spectra in Fig. 3a, where the sample was first cooled to 232 K (23 K below eutectic) and then warmed to 246 K (9 K below eutectic), show a dominant absorption feature between 1081-1084 eV clearly resembling the features in the reference spectrum of aqueous $NaNO_3$ solutions (Fig. 2). Precipitation of $NaNO_3$ did not occur. The presence of aqueous $NaNO_3$ shows that either the sample did not nucleate at 232 K (23 K below eutectic) and remained in the liquid phase upon warming to 246 K, or alternatively, it may have remained solvated within a liquid-like environment at the air-ice interface (referred to as 'quasi-brine' by Cho et al. (2002)). Here we use ‘aqueous-like’ to refer to both supercooled interfacial brine and solvation environments in the liquid-like layer of ice, which we do not attempt to distinguish spectroscopically. Clearly, sodium of $NaNO_3$ in the presence of ice stays in supercooled solutions or forms liquid-like hydrogen bonds with water molecules on ice at temperatures down to 23 K below the eutectic.

https://doi.org/10.5194/egusphere-2026-3716
Preprint. Discussion started: 27 July 2026


To further investigate the role of ice, spectra were acquired below the eutectic in the absence of ice. First, the sample was cooled, in absence of ice, to 243 K (12 K below eutectic), then warmed above the eutectic and cooled again to 248 K (7 K below eutectic) and finally warmed to 253 K for the final NEXAFS acquisition. Figure 3b shows these Na K-edge NEXAFS spectra with two prominent absorption features between 1079-1081 eV and 1083-1086 eV. These two features remain relatively constant with changes in temperatures. Comparing the spectra to the references in Fig. 2, we conclude that these are characteristic for crystalline $NaNO_3$, the minor deviation in the ratio of the two features to published data is consistent with instrumental artifacts and with grain orientation as described above. Note that, at room temperature, $NaNO_3$ has a rhombohedral structure (Phase I, R3c; "nitratine"). The order to disorder transition occurs ~ 550 K. Therefore, even though $NaNO_3$ is a polymorph, there is no indication that at lower temperatures a different crystal structure does form that might explain the minor deviations. A further hypothesis is that different crystal facets might be probed (Preobrajenski et al., 2002). As facets differ in their interfacial structure, this might be reflected in the NEXAFS. The research about different crystal facets of $NaNO_3$ at cold temperatures was beyond the scope of this study and needs further investigation. In summary, Fig. 3b clearly showed that $NaNO_3$ crystallized in the absence of ice. This finding is different to the outcome presented above of $NaNO_3$ with ice, where NEXAFS spectra taken for temperatures at 232 K to 246 K indicated an aqueous-like first hydrogen bonding shell of sodium. To probe the chemical environment of nitrate in this ice-free experiment, Nitrogen K-edge NEXAFS spectra were acquired. These show a sharp absorption feature at 405 eV photon energy and a broad feature from 410 eV to 420 eV (Fig. 4). Due to the absorption of the incoming X-ray in the N K-edge region prior to hitting the sample, the absolute number of counts in this region was low, and the resulting spectra show a lower signal to noise ratio than the sodium spectra. Nevertheless, one might tentatively identify a double feature characteristic for crystalline $NaNO_3$ (Smith et al., 2015) in the reference spectrum (Fig. 4 light red line) and a single, broader peak as observed in nitrate solutions (Smith et al., 2015) in humid condition above the eutectic (Fig. 4 light blue line). Then, the two N K-edge NEXAFS spectra below the eutectic are consistent with the conclusion of crystalline $NaNO_3$ present in these samples. The relatively modest contrast between the N K-edge spectra of crystalline and dissolved nitrate, compared to the clear distinction seen in the Na K-edge data, reflects an intrinsic geometric limitation: the nitrogen atom in $NO_3^-$ is always coordinated by its three equivalent oxygen ligands, which dominate the near-edge structure and screen the nitrogen from direct sensitivity to the outer solvation shell (Preobrajenski et al., 2004) whether that shell consists of hydrogen-bonded water molecules or sodium counterions.

Results of the experiments presented in Fig. 3 indicate a different behavior for $NaNO_3$ brine in the presence and absence of ice. Nucleation of $NaNO_3$ did not occur on the air-ice interface. Photographs of the samples give further insights: The pictures of the sample without ice do not indicate the growth of a thick or visible layer of ice on or around the nitrate salt as visible in Fig. 5b. The images show the sample with a whitish color and a clear border, meaning that the sample was not covering the entire sample plate. The presence of ice is usually indicated with a certain shininess and a broader coverage of the sample plate with the ice, as visible in Fig. 5a. Clearly evident is the growth of crystallized $NaNO_3$ with a clear border for the crystal as visible in the image shown in Fig. 5b.

https://doi.org/10.5194/egusphere-2026-3716
Preprint. Discussion started: 27 July 2026


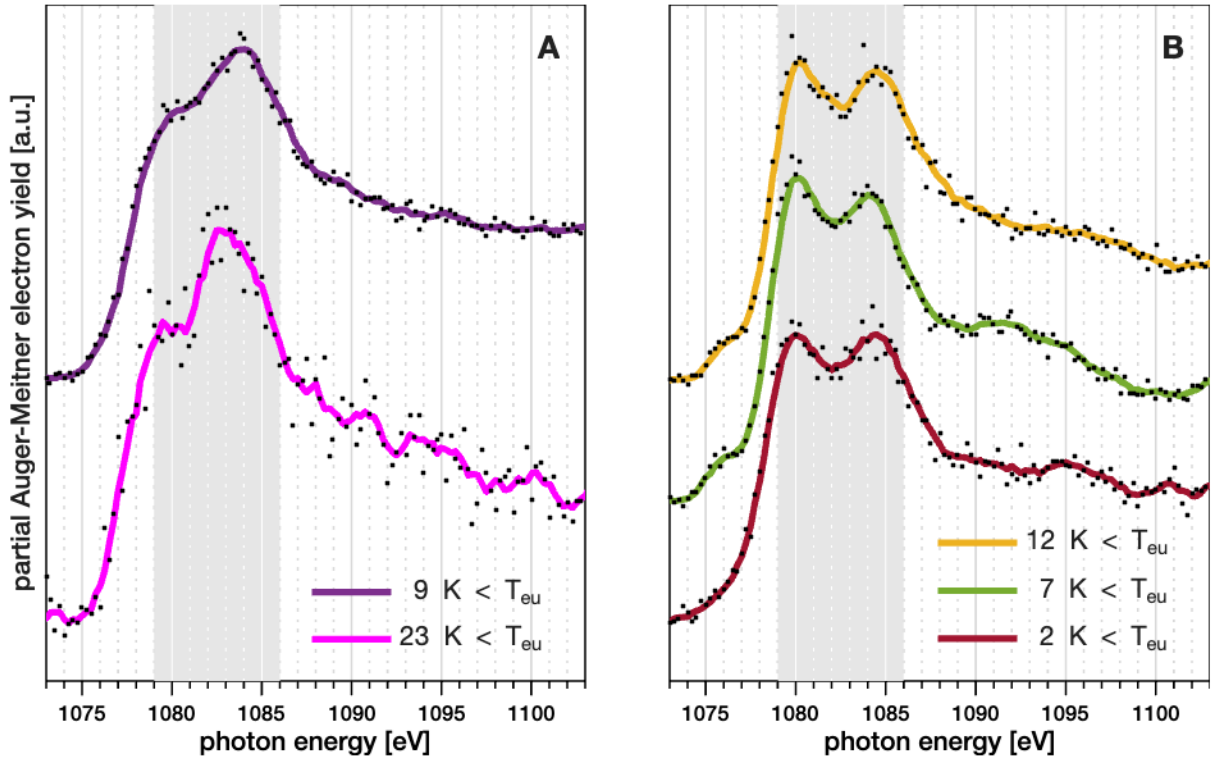


**Figure 3: In panel A, Na K-edge NEXAFS spectra acquired on $NaNO_3$ in presence of ice at 246 K (dark purple line) and at 232 K (light purple line) are shown. Sodium K-edge NEXAFS spectra acquired on $NaNO_3$ without ice at 243 K (yellow line), 248 K (green line) and 253 K (dark red line) are shown in panel B. The temperature difference to the eutectic point is indicated in the legend. Lines and black dots are the same as in Fig. 2.**

https://doi.org/10.5194/egusphere-2026-3716
Preprint. Discussion started: 27 July 2026


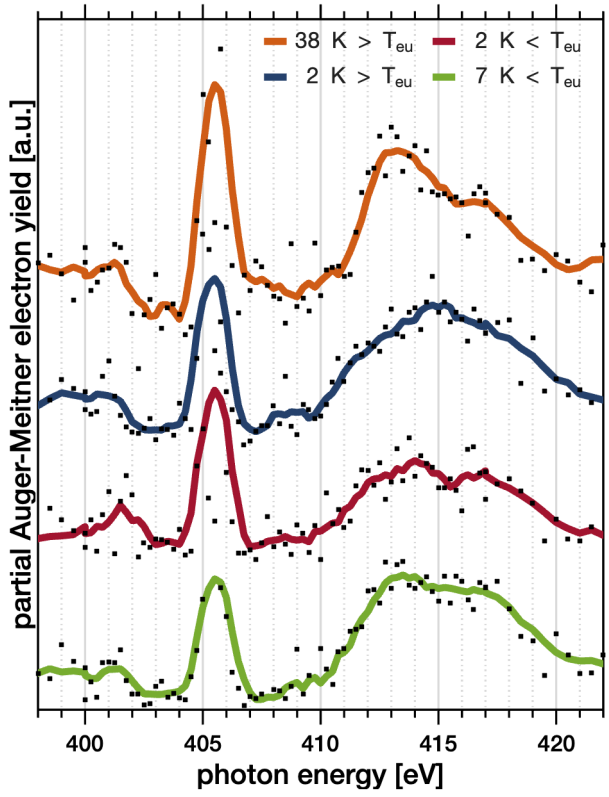


**Figure 4: Nitrogen K-edge NEXAFS spectra of solid $NaNO_3$ acquired at a RH of 3.5% (light red), of aqueous sodium nitrate in presence of ice above the eutectic (dark blue), and at two temperatures below the eutectic point with identical settings to those in Fig. 3b (green and dark red lines). The spectra were plotted stacked on top of each other for comparison reasons, with the photon energy on the x-axis and the normalized intensity (partial Auger-Meitner electron counts) on the y-axis.**

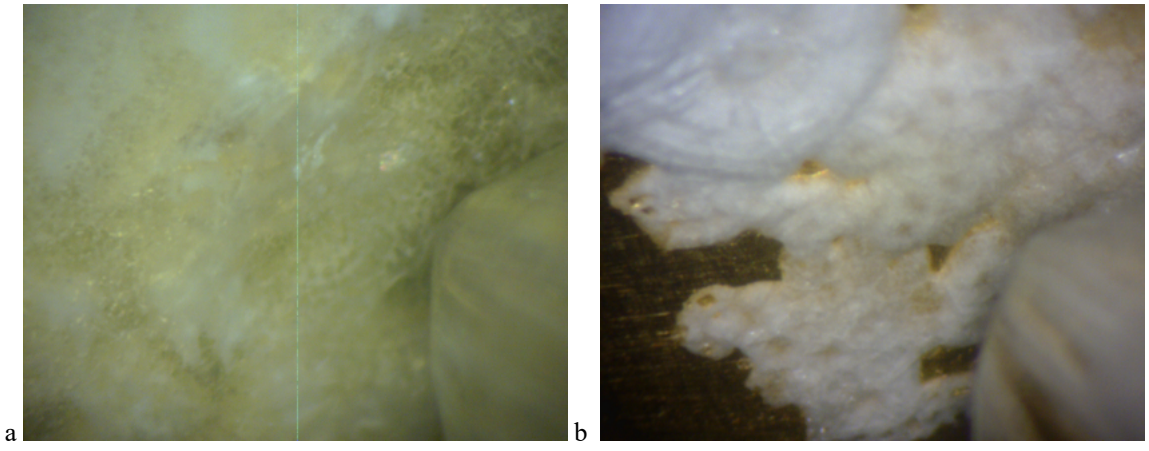


**Figure 5: Image of $NaNO_3$ samples in presence of ice at 9 K below the eutectic, prior to the acquisition of the NEXAFS spectrum presented in Fig. 3a (purple line). An image of $NaNO_3$ in the absence of ice at 2 K below the eutectic is shown in b. NEXAFS spectrum of the sample in b is shown in Fig. 3b (dark red line).**

https://doi.org/10.5194/egusphere-2026-3716
Preprint. Discussion started: 27 July 2026


### 3.3 Phase state controls the $NO_2$ to HONO photolysis ratio

Having established spectroscopically that nitrate retains aqueous-like solvation at ice surfaces down to 232 K (Sect. 3.2), we now directly probe the consequences. For this, the $NO_2$ and HONO emissions into a carrier gas passing porous snow samples were monitored above and below the eutectic temperature of sodium nitrate (Fig. 6). At 258 K, when the sodium nitrate forms aqueous brine solutions embedded in snow, the response to the irradiation at 0 min. is fast. Mixing ratio of $NO_2$ and of HONO in the carrier gas exiting the porous snow increase rapidly within 5 minutes to a (nearly) stable level. The emissions into the carrier gas from nitrate in snow at UVB irradiation level off at 190 ppb ($NO_2$) and 6 ppb (HONO) at 253 K and 750 ppb ($NO_2$) and 91 ppb (HONO) at 258 K. Irradiated with UVB and UVA, snow emits 62 ppb ($NO_2$) and 2 ppb (HONO) at 253 K and 430 ppb ($NO_2$) and 35 ppb (HONO) at 258 K. Absolute emissions are generally reduced from snow with precipitated nitrate with $NO_2$ decreasing by one third. Interestingly, the shape of the $NO_2$ emission profile with time changes upon precipitation, where the emissions can be described by both a slower increase and decline. HONO emissions with UVB and UVA irradiation were close to detection limit making interpretation of the emission with time and its mixing ratio uncertain. The $NO_2$ emissions from three (two) repeated experiments with new snow samples each at 253 K and UVB (UVB and UVA) irradiation range between 91 ppb and 265 ppb (24 ppb and 91 ppb) and show the reproducibility. Factors influencing the emissions are differences in the snowpack density and potential localization of the nitrate within the snow (Bartels-Rausch et al., 2014). In the following, we discuss the $NO_2$:HONO emission ratio, which is about 8 with UVB light (Fig. 6A) and about 13 with UVB and UVA light combined (Fig. 6B) at 258 K. At 253 K, where sodium nitrate remained precipitated, the ratio increases to about 30 (UVB, Fig. 6A; UVA and B, Fig 6. B). Note that in these experiments samples were frozen to 77 K to ensure precipitation of $NaNO_3$ prior to warming to the experimental temperatures mentioned above.

$$NO_2^- + h\nu\ (UVA)(+H^+) \rightarrow NO\ + OH \qquad \text{(Eq. 3)}$$

$$NO_2^- + OH \rightarrow NO_2\ + OH^- \qquad \text{(Eq. 4)}$$

The primary quantum yields ratio of Eq. 1 and Eq. 2 have been extensively investigated and recent laboratory work showed a ratio in the primary quantum yields of photolysis channel 1 (Eq. 1) and channel 2 (Eq. 2) and thus a primary $NO_2$ to HONO ratio of 1:1, while earlier work suggested a ratio of 10:1 (Benedict et al., 2017; Goldstein and Rabani, 2007; McFall et al., 2018b; Warneck and Wurzinger, 1988). A complex chemistry of the primary photolysis products nitrite and $NO_2$ is well known (Eqs. 3 and 4). Benedict et al. (2017) showed how the differences in experimental settings such as concentration of nitrate, presence of organics or $CO_2$ as OH scavengers, temperature, and irradiation wavelength impact these secondary reactions, the observed product ratio, and thus reported quantum yields. While the impact of secondary reactions must be minimized in studies determining the primary quantum yield, Jacobi et al. (2014) showed how these reactions impact emissions from natural snow. They found nitrite photochemistry (Eq. 3) a stronger NOx source than the nitrate photolysis in snow samples from Alaska. While investigating the role of secondary chemistry in snow is the scope of ongoing work involving a snow-chemistry

https://doi.org/10.5194/egusphere-2026-3716
Preprint. Discussion started: 27 July 2026


transport model (Kuhn et al., 2025), here we qualitatively probed the impact of changes in the irradiation wavelength on the product distribution. Clearly, our results show how the overall yields of HONO relative to $NO_2$ are slightly suppressed in aqueous nitrate brine compared to the results by Benedict and Anastasio (2017). Temperature cannot explain the higher yield of $NO_2$ in our experiments as at lower temperatures Eq. 2 forming nitrite dominates. At 258 K, Benedict and Anastasio (2017) found a $NO_2$ to HONO ratio of 0.75, reflection both changes of cross section with temperature and of the primary quantum yield with concentration. Note that the experiments by Benedict and Anastasio (2017) are similar to ours in sample concentration as both investigated brine mixtures embedded in a frozen matrix. Thermodynamics of the freezing point depression dictate sodium nitrate concentrations of approximately 4 M during both experiments. Adding UVA irradiation further enhances the $NO_2$ emission relative to that of HONO, and precipitation of nitrate strongly enhances the $NO_2$ to HONO emission ratio. Nitrate absorption is essentially confined to the UVB range (Fig. 7, yellow dashed line), so the primary photolysis channels (Eqs. 1 and 2) proceed with comparable yields. Nitrite absorbs efficiently in the UVA (Fig. 7, red dashed line), meaning that the addition of UVA radiation selectively accelerates secondary nitrite photolysis (Eq. 3). This consumes nitrite within the snowpack and thus shifts the $NO_2$ to HONO emission ratio upward relative to UVB irradiation alone. Subsequent reaction of nitrite with OH (Eq. 4), produced both by nitrate (Eq. 1) and nitrite (Eq. 3) photolysis, shift the emission ratio further to $NO_2$. Figure 6 shows the enhancement is stronger for brine, where the aqueous secondary chemistry of Eqs. 3 and 4 operates efficiently, than for precipitated nitrate.

https://doi.org/10.5194/egusphere-2026-3716
Preprint. Discussion started: 27 July 2026


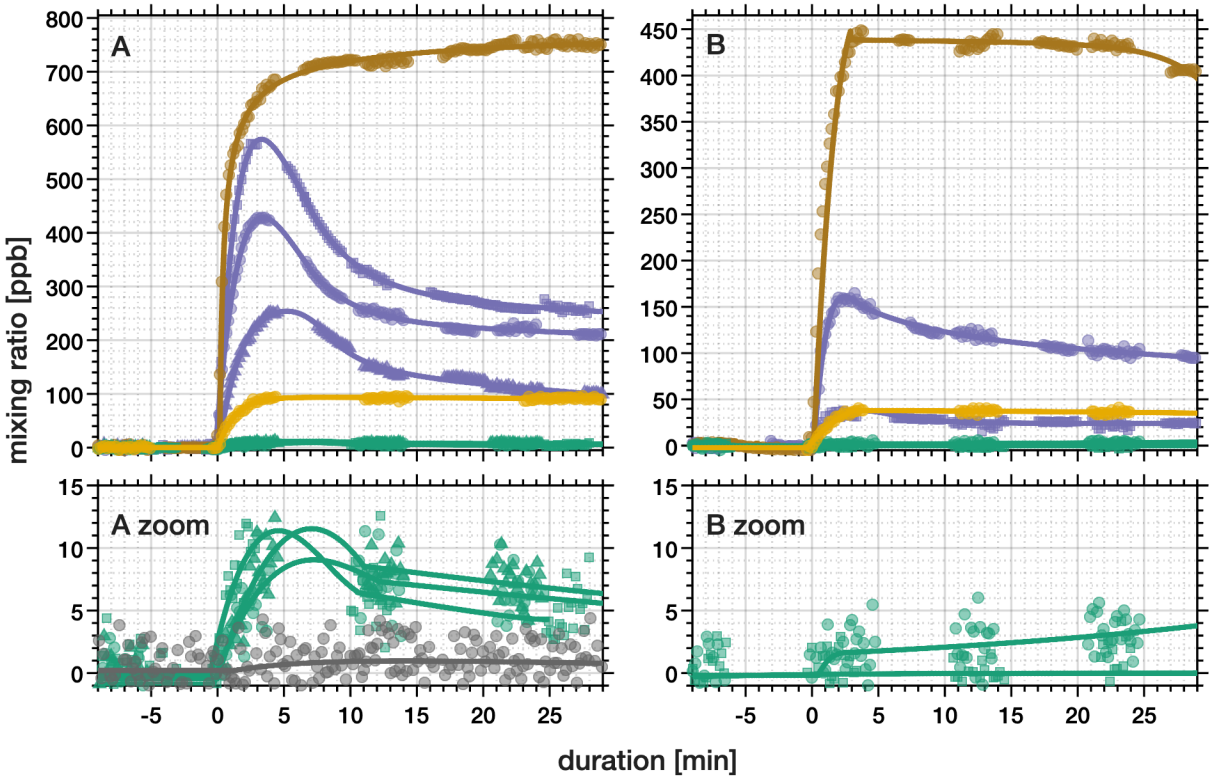


**Figure 6: Nitrogen oxide emission from photolysis of snow with sodium nitrate brine at 258 K (brown and yellow) and precipitated salt at 253 K(violet and green). The y-axis gives the mixing ratio of $NO_2$ (brown and violet) and of HONO (yellow and green) in the carrier gas flow of 125 mL/min STP passing through the snow. Irradiation with UVB (A) or UVA and UVB (B) started at 0 minutes and lasted for 30 minutes. The lower graph provides a detailed view of HONO emissions originating from precipitated salt in snow, including results from a snow sample without nitrate doping (displayed in grey). Data points are represented by markers, while lines serve as visual guides. Gas flow from the snow sample was alternated between different analyzers causing the gaps in data.**

https://doi.org/10.5194/egusphere-2026-3716
Preprint. Discussion started: 27 July 2026


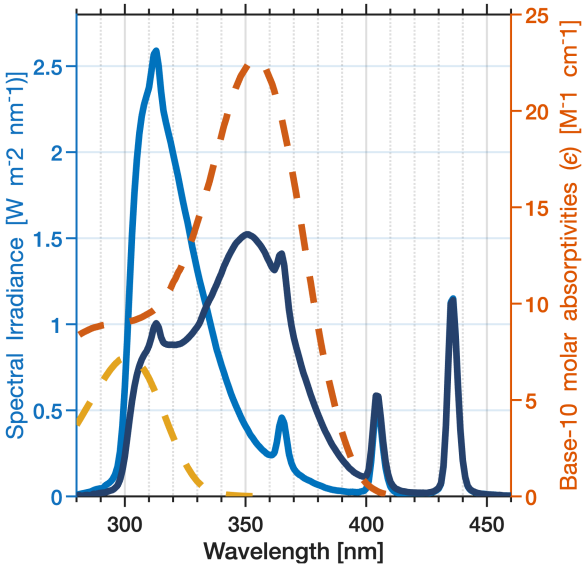


**Figure 7: Spectral Irradiance at the sample position for UVB (light blue) and UVA/UVB (dark blue) irradiation and the base-10 molar absorptivity of nitrate (yellow dashed line) (Chu and Anastasio, 2003) and of nitrite (red dashed line) (Chu and Anastasio, 2007) in aqueous solution at 274 K or 278 K, respectively.**

## 4 Conclusions

The solid and aqueous phases of $NaNO_3$ were successfully characterized by means of KLL-transitions in the Na K-edge NEXAFS spectra. Cooling down the $NaNO_3$ brine with and without ice to temperatures below the eutectic led to different outcomes, such as the detection of the solid phase or an aqueous $NaNO_3$ solution. Previously, mixtures of solid nitrate and aqueous nitrate solution at the ice surface close to the eutectic temperature were found by Morenz and Donaldson (2017) using Raman microscopy. Morenz and Donaldson (2017) detected a large variation in the nitrate distribution across the horizontal extent of ice samples, and concluded that nitrate congregates in pockets or grain boundaries, where nitrate experiences a solution-like environment in pockets and forms solid crystals at the surface. Kahan et al. (2014b) also investigated the structure of the air-ice interface upon freezing of salt solutions with a probing depth of tens to hundreds of water layers and concluded that nitrate is excluded to the air-ice interface during freezing. They state that the low surface concentration of nitrate suggests that it prefers to remain in liquid pockets or other interfacial regions within the bulk. Marrocco and Michelsen (2014) tried to quantify the amount of liquid in frozen samples of $NaNO_3$, and they pointed out the low solubility of nitrate in the ice, and that nitrate is therefore unlikely within the ice lattice but rather trapped in liquid channels or networks upon freezing. The lack of a solid phase detected in presence of ice in our experiments (Fig. 3) can however not be due to detecting only pockets and grain boundaries within the measured spot. This would require heterogeneities (surface patches of aqueous phase) larger than 300 $\mu m^2$, which is the spot size of the X-ray beam.

https://doi.org/10.5194/egusphere-2026-3716
Preprint. Discussion started: 27 July 2026


Koop et al. (2000) demonstrated how the concentrations of ions present in the liquid fraction of frozen systems increase strongly with decreasing temperature. This can result in a rise of reaction rates (Takenaka et al., 1992). Grannas et al. (2007) showed such an enhancement of the reaction rate by a factor of 40 for the photochemical reaction of organics in ice compared to the aqueous phase. The presence of sodium nitrate either in a supercooled solution or in an aqueous-like environment in the interfacial region of ice at the temperatures significantly below the eutectic (as 23 K < $T_{eu}$) has implications on the reactivity of the salt at the interface in snow and ice. Photolysis experiments show marked differences in the photolysis emission ratio of $NO_2$ to HONO for nitrate brine and nitrate crystals at the interstitial snow surface. A liquid-like or liquid interfacial reservoir favors enhanced HONO formation relative to $NO_2$, whereas precipitated nitrate exhibits reduced reactivity and a markedly higher $NO_2$ to HONO emission ratio. This is consistent with the framework established by McFall et al. (2018a) and Chan et al. (2025) that the hydrogen-bond solvation environment around nitrate and not temperature *per se*, governs both the primary quantum yield branching ratio and secondary chemistry. The single Arrhenius relationship in LLR ice reported by Benedict and Anastasio (2017), showing no discontinuity at the $NaNO_3$ eutectic, reflected the persistence of liquid-like solvation in those experiments; the present NEXAFS measurements provide direct spectroscopic evidence that this solvation persists at ice surfaces down to 232 K, and the snow photolysis experiments show its photochemical consequences. Jacobi et al. (2014) demonstrated in the field that nitrite can contribute more to boundary-layer $NO_x$ through photolysis than nitrate photolysis itself; the present findings suggest that the efficiency of this entire cascade depends on whether nitrate is in a liquid-like or crystalline state, currently not represented in snowpack photochemistry models.

The temperature dependence reported by Benedict and Anastasio (2017) follows the single Arrhenius relationship, which predicts that at 258 K the primary quantum yield for Channel 2 already exceeds that for Channel 1, with the $NO_2$ to nitrite primary ratio being approximately 0.75. Chan et al. (2025) rationalize this through a rearrangement of hydrogen bonds to nitrate. At 258 K, the energy requirement for forming a solvation-shell required by Channel 1 suppresses it relative to Channel 2. The apparent $NO_2$ to HONO emission ratio of ~13 measured here from brine reflects the secondary reduction of HONO emissions from the snowpack, through photolysis of accumulated nitrite and oxidation of nitrite by OH. The relatively long residence time of HONO adsorbed on the large internal surface of snow (Bartels et al., 2002; Kerbrat et al., 2010) increases its photolysis probability. The strong suppression of HONO emission observed here when nitrate crystallizes, relative to brine under otherwise identical conditions, reflects not a temperature effect but a change in phase: Crystallization removes the liquid-like solvation environment that supports an efficient secondary chemistry.

Including the interfacial nitrate photolysis of aerosol in current GEOS-Chem implementations has greatly improved the simulated vs. observed nitrogen oxide budgets (Rowlinson et al., 2025; Shah et al., 2023). Both implementations differ in the photolysis rate, parameterized as enhancement factor relative to the gas-phase photolysis of $HNO_3$, but share the same branching ratio of $NO_2$ vs. HONO production of 0.66. Rowlinson et al. (2025) showed a reduced model HONO bias in remote

https://doi.org/10.5194/egusphere-2026-3716
Preprint. Discussion started: 27 July 2026


tropospheric campaigns. This simulated global NOx source was found comparable to the anthropogenic NOx emissions combined and pushed ozone and OH beyond observational constraints. While these global models show the large scale importance of nitrate emissions for the global NOy budget, they also call for better constraints on photolysis yields and branching ratios. Solid or crystalline nitrate (as would form at temperatures below the eutectic without ice present) should produce less HONO per photon than liquid-phase or supercooled brine, a distinction current model parameterizations do not capture. Li et al. (2024) demonstrated that phase state regulates photochemical HONO production in $NaNO_3$ dicarboxylic acid aerosol mixtures, with HONO production rates increasing by roughly an order of magnitude as particles transitioned from solid to liquid state with rising relative humidity. This is consistent with the present finding that aqueous-like nitrate in snow produces more HONO than crystalline $NaNO_3$ and supports this phase-state dependence of HONO yields across atmospheric condensed phases.

Bond et al. (2023) showed that snowpack nitrate photolysis drives the summertime HONO budget in coastal Antarctica by an order of magnitude over gas-phase sources. The eutectic of $NaNO_3$ is 255 K meaning that coastal Antarctic summer snowpacks should frequently be in the temperature range where, as this study shows, nitrate remains in a liquid-like state. Bond et al. (2023) quantify the HONO production rate from direct nitrate photolysis using a yield of 10%, derived from the ice-phase quantum yields of Chu and Anastasio (2003), and find this closely capturing the observed fluxes. The snow photolysis experiments presented here now call for the possibility of lower HONO fluxes from potentially precipitated nitrate and enhanced secondary chemistry within the snowpacks.

Beyond its implications for boundary layer HONO budgets from snowpack emissions, the nitrate photochemistry described here also has implications for the interpretation of ice-core nitrate records. Inverse models that use ice-core nitrate isotope profiles to reconstruct primary nitrate deposition fluxes and their $\delta^{15}N$ and $\Delta^{17}O$ signatures (Jiang et al., 2024) rely on two parameters that are directly sensitive to the phase state of interfacial nitrate. The photolysis quantum yield ($\Phi$), which controls how much nitrate is photolyzed as a function of actinic flux; and the cage-effect fraction (fc), which captures the extent of secondary chemistry that exchanges oxygen isotopes with snow water and thereby modulates the $\Delta^{17}O$ signal, are both currently treated as climate-invariant calibration constants. The present finding that liquid-like nitrate supports substantially more secondary chemistry than crystalline nitrate implies that fc, in particular, should be higher under conditions where nitrate remains in a liquid-like interfacial state, and lower where crystallization becomes relevant. For present-day polar summer conditions, which remain above 232 K, the calibrated values likely implicitly reflect liquid-like chemistry and are broadly appropriate. However, for periods when East Antarctic summer surface temperatures were several degrees colder, the possible approach toward the phase-transition boundary would imply systematically reduced fc introducing biases in the reconstructed primary nitrate flux and its isotopic composition that are not be identified by any isotopic constraint alone.

https://doi.org/10.5194/egusphere-2026-3716
Preprint. Discussion started: 27 July 2026


## Author contribution

Conceptualization: TBR. Data Curation: YM, ZG, TBR. Funding Acquisition: TBR. Supervision: TBR. Formal Analysis, Validation, and Visualization: YM, ZG, TBR. Investigation: YM, ZG, JPG, LA, MA, AB; TBR. Methodology: JPG, YM, ZG, MA, LA, TBR. Software: TBR. Writing, original draft: YM, ZG, MA, TBR. Writing, review and editing: all authors.

## Competing interests

At least one of the (co-)authors is a member of the editorial board of Atmospheric Chemistry and Physics.

## Acknowledgement

The technical support by Andrés Laso is highly appreciated. We thank the staff of PSI/SLS for excellent beam quality and the beamline scientists at ISS and SIM for their support. Part of this work was carried out as part of the doctoral dissertation by YM at the ETHZ. YM thanks Peter Alpert for fruitful discussions. TBR acknowledges the use of Copilot and Claude (accessed in April to June 2026) to support in language polishing. All AI-generated suggestions were reviewed, revised, and approved by the authors, who take full responsibility for the accuracy and integrity of the work.

## Financial support.

This work was supported by the Swiss National Science Foundation (Grant 178 962).

## Data Availability

Data is available at the EnviDat repository: Manoharan, Y., Golay, Z., Bartels-Rausch, T. (2026) Laboratory Dataset on the photolysis and phase change of sodium nitrate at the air-ice interface. https://www.doi.org/10.16904/envidat.763

## References

Aduru, S., Contarini, S., and Rabalais, J. W.: Electron-, x-ray-, and ion-stimulated decomposition of nitrate salts, J. Phys. Chem., 90, 1683–1688, https://doi.org/10.1021/j100399a045, 1986.

Ammann, M., Artiglia, L., and Bartels-Rausch, T.: X-Ray Excited Electron Spectroscopy to Study Gas–Liquid Interfaces of Atmospheric Relevance, 135–166, 2018.

Andersen, S. T., Carpenter, L. J., Reed, C., Lee, J. D., Chance, R., Sherwen, T., Vaughan, A. R., Stewart, J., Edwards, P. M., Bloss, W. J., Sommariva, R., Crilley, L. R., Nott, G. J., Neves, L., Read, K., Heard, D. E., Seakins, P. W., Whalley, L. K., Boustead, G. A., Fleming, L. T., Stone, D., and Fomba, K. W.: Extensive field evidence for the release of HONO from the photolysis of nitrate aerosols, Sci. Adv., 9, eadd6266, https://doi.org/10.1126/sciadv.add6266, 2023.

https://doi.org/10.5194/egusphere-2026-3716
Preprint. Discussion started: 27 July 2026


Armstrong, B. I., Copeland, A. D., Donadio, D., and Raiteri, P.: Pseudo-grand canonical molecular dynamics via volumetrically controlled osmotic pressure, J. Chem. Phys., 163, 114102, https://doi.org/10.1063/5.0287608, 2025.

Aziz, E. F., Zimina, A., Freiwald, M., Eisebitt, S., and Eberhardt, W.: Molecular and electronic structure in NaCl electrolytes of varying concentration: Identification of spectral fingerprints, J. Chem. Phys., 124, 114502, https://doi.org/10.1063/1.2176616, 2006.

Bartels, T., Eichler, B., Zimmermann, P., Gäggeler, H. W., and Ammann, M.: The adsorption of nitrogen oxides on crystalline ice, Atmospheric Chem. Phys., 2, 235–247, https://doi.org/10.5194/acp-2-235-2002, 2002.

Bartels-Rausch, T., Guimbaud, C., Gäggeler, H. W., and Ammann, M.: The partitioning of acetone to different types of ice and snow between 198 and 223 K, Geophys. Res. Lett., 31, https://doi.org/https://doi.org/10.1029/2004GL020070, 2004.

Bartels-Rausch, T., Jacobi, H. W., Kahan, T. F., Thomas, J. L., Thomson, E. S., Abbatt, J. P. D., Ammann, M., Blackford, J. R., Bluhm, H., Boxe, C., Domine, F., Frey, M. M., Gladich, I., Guzmán, M. I., Heger, D., Huthwelker, T., Klán, P., Kuhs, W. F., Kuo, M. H., Maus, S., Moussa, S. G., McNeill, V. F., Newberg, J. T., Pettersson, J. B. C., Roeselová, M., and Sodeau, J. R.: A review of air–ice chemical and physical interactions (AICI): liquids, quasi-liquids, and solids in snow, Atmos Chem Phys, 14, 1587–1633, https://doi.org/10.5194/acp-14-1587-2014, 2014.

Bartels-Rausch, T., Kong, X., Orlando, F., Artiglia, L., Waldner, A., Huthwelker, T., and Ammann, M.: Interfacial supercooling and the precipitation of hydrohalite in frozen NaCl solutions as seen by X-ray absorption spectroscopy, The Cryosphere, 15, 2001–2020, https://doi.org/10.5194/tc-15-2001-2021, 2021.

Bartels-Rausch, T., Creamean, J., Thomas, J. L., Willis, M., and Zieger, P.: Ten crucial unknowns in atmospheric chemistry in the cold, Faraday Discuss., 258, 10–22, https://doi.org/10.1039/D5FD00056D, 2025.

Benedict, K. B. and Anastasio, C.: Quantum yields of nitrite ($NO_2^-$) from the photolysis of nitrate ($NO_3^-$) in ice at 313 nm, J. Phys. Chem. A, 121, 8474–8483, https://doi.org/10.1021/acs.jpca.7b08839, 2017.

Benedict, K. B., McFall, A. S., and Anastasio, C.: Quantum yield of nitrite from the photolysis of aqueous nitrate above 300 nm, Environ. Sci. Technol., 51, 4387–4395, https://doi.org/10.1021/acs.est.6b06370, 2017.

Berrens, M. L., Chen, Z., Chan, K.-T., Anastasio, C., and Donadio, D.: Solvation structure and UV–visible absorption spectra of the nitrate anion at the air–ice interface by first-principles molecular simulations, ACS Earth Space Chem., 7, 1761–1769, https://doi.org/10.1021/acsearthspacechem.3c00127, 2023.

Blaszczak-Boxe, C. S. and Saiz-Lopez, A.: Nitrate photolysis in ice and snow: A critical review of its multiphase chemistry, Atmos. Environ., 193, 224–241, https://doi.org/10.1016/j.atmosenv.2018.09.002, 2018.

Bond, A. M. H., Frey, M. M., Kaiser, J., Kleffmann, J., Jones, A. E., and Squires, F. A.: Snowpack nitrate photolysis drives the summertime atmospheric nitrous acid (HONO) budget in coastal Antarctica, Atmos Chem Phys, 23, 5533–5550, https://doi.org/10.5194/acp-23-5533-2023, 2023.

Bridgeman, O. C. and Aldrich, E. W.: Vapor pressure tables for water, J. Heat Transf., 86, 279–286, https://doi.org/10.1115/1.3687121, 1964.

Chan, K.-T., Berrens, M. L., Chen, Z., McCurdy, C. W., Anastasio, C., and Donadio, D.: Revealing the photochemical pathways of nitrate in water through first-principles simulations, J. Chem. Phys., 162, 144318, https://doi.org/10.1063/5.0262438, 2025.

https://doi.org/10.5194/egusphere-2026-3716
Preprint. Discussion started: 27 July 2026


Chen, C. T., Ma, Y., and Sette, F.: K-shell photoabsorption of the $N_2$ molecule, Phys. Rev. A, 40, 6737–6740, https://doi.org/10.1103/PhysRevA.40.6737, 1989.

Cheng, P., Ma, W., Yu, Y., Li, H., Huang, L., Ling, J., Yang, W., Tian, Z., Yu, X., Ma, N., Kuang, Y., Zhang, S., Xu, W., Zhao, H., Zhang, G., Tan, Z., Huang, Z., Fu, P., Su, H., and Cheng, Y.: Snow-induced perturbations in nitrous acid (HONO) levels: Insights into heterogeneous reactions during wintertime in mid-latitude regions, Geophys. Res. Lett., 52, e2024GL113896, https://doi.org/10.1029/2024GL113896, 2025.

Cho, H., Shepson, P. B., Barrie, L. A., Cowin, J. P., and Zaveri, R.: NMR investigation of the quasi-brine layer in ice/brine mixtures, J. Phys. Chem. B, 106, 11226–11232, https://doi.org/10.1021/jp020449+, 2002.

Chu, L. and Anastasio, C.: Quantum yields of hydroxyl radical and nitrogen dioxide from the photolysis of nitrate on ice, J. Phys. Chem. A, 107, 9594–9602, https://doi.org/10.1021/jp0349132, 2003.

Chu, L. and Anastasio, C.: Temperature and wavelength dependence of nitrite photolysis in frozen and aqueous solutions, Environ. Sci. Technol., 41, 3626–3632, https://doi.org/10.1021/es062731q, 2007.

De Wispelaere, S., Cabaret, D., Levelut, C., Rossano, S., Flank, A.-M., Parent, P., and Farges, F.: Na-, Al-, and Si K-edge XANES study of sodium silicate and sodium aluminosilicate glasses: influence of the glass surface, Chem. Geol., 213, 63–70, https://doi.org/10.1016/j.chemgeo.2004.08.033, 2004.

Edebeli, J., Trachsel, J. C., Avak, S. E., Ammann, M., Schneebeli, M., Eichler, A., and Bartels-Rausch, T.: Snow heterogeneous reactivity of bromide with ozone lost during snow metamorphism, Atmospheric Chem. Phys., 20, 13443–13454, https://doi.org/10.5194/acp-20-13443-2020, 2020.

Frey, M. M., Savarino, J., Morin, S., Erbland, J., and Martins, J. M. F.: Photolysis imprint in the nitrate stable isotope signal in snow and atmosphere of East Antarctica and implications for reactive nitrogen cycling, Atmos Chem Phys, 9, 8681–8696, https://doi.org/10.5194/acp-9-8681-2009, 2009.

Galib, M., Baer, M. D., Skinner, L. B., Mundy, C. J., Huthwelker, T., Schenter, G. K., Benmore, C. J., Govind, N., and Fulton, J. L.: Revisiting the hydration structure of aqueous $Na^+$, J. Chem. Phys., 146, 084504, https://doi.org/10.1063/1.4975608, 2017.

Gen, M., Liang, Z., Zhang, R., Go, B. R., and Chan, C. K.: Particulate nitrate photolysis in the atmosphere, Environ. Sci. Atmospheres, 2, 111–127, https://doi.org/10.1039/D1EA00087J, 2022.

Goldstein, S. and Rabani, J.: Mechanism of nitrite formation by nitrate photolysis in aqueous solutions: the role of peroxynitrite, nitrogen dioxide, and hydroxyl radical., J. Am. Chem. Soc., 129, 10597–10601, https://doi.org/10.1021/ja073609+, 2007.

Gopakumar, G., Muchová, E., Unger, I., Malerz, S., Trinter, F., Öhrwall, G., Lipparini, F., Mennucci, B., Céolin, D., Caleman, C., Wilkinson, I., Winter, B., Slavíček, P., Hergenhahn, U., and Björneholm, O.: Probing aqueous ions with non-local Auger relaxation, Phys. Chem. Chem. Phys., 24, 8661–8671, https://doi.org/10.1039/D2CP00227B, 2022.

Grannas, A. M., Bausch, A. R., and Mahanna, K. M.: Enhanced aqueous photochemical reaction rates after freezing, J. Phys. Chem. A, 111, 11043–11049, https://doi.org/10.1021/jp073802q, 2007.

Hullar, T., Tran, T., and Anastasio, C.: Nitrate photolysis at the air–ice interface of nature-identical snow, ACS Earth Space Chem., 7, 1791–1797, https://doi.org/10.1021/acsearthspacechem.3c00166, 2023.

https://doi.org/10.5194/egusphere-2026-3716
Preprint. Discussion started: 27 July 2026


Jacobi, H.-W., Kleffmann, J., Villena, G., Wiesen, P., King, M., France, J., Anastasio, C., and Staebler, R.: Role of nitrite in the photochemical formation of radicals in the snow, Environ. Sci. Technol., 48, 165–172, https://doi.org/10.1021/es404002c, 2014.

Jiang, Z., Alexander, B., Savarino, J., and Geng, L.: An inverse model to correct for the effects of post-depositional processing on ice-core nitrate and its isotopes: model framework and applications at Summit, Greenland, and Dome C, Antarctica, Atmos Chem Phys, 24, 4895–4914, https://doi.org/10.5194/acp-24-4895-2024, 2024.

Kahan, T. F., Wren, S. N., and Donaldson, D. J.: A Pinch of Salt Is All It Takes: Chemistry at the Frozen Water Surface, Acc. Chem. Res., 47, 1587–1594, https://doi.org/10.1021/ar5000715, 2014a.

Kahan, T. F., Wren, S. N., and Donaldson, D. J.: A pinch of salt is all it takes: Chemistry at the frozen water surface, Acc. Chem. Res., 47, 1587–1594, https://doi.org/10.1021/ar5000715, 2014b.

Kerbrat, M., Huthwelker, T., Bartels-Rausch, T., Gäggeler, H. W., and Ammann, M.: Co-adsorption of acetic acid and nitrous acid on ice, Phys Chem Chem Phys, 12, 7194–7202, https://doi.org/10.1039/B924782C, 2010.

Kong, X., Waldner, A., Orlando, F., Artiglia, L., Huthwelker, T., Ammann, M., and Bartels-Rausch, T.: Coexistence of physisorbed and solvated HCl at warm ice surfaces, J. Phys. Chem. Lett., 8, 4757–4762, https://doi.org/10.1021/acs.jpclett.7b01573, 2017.

Kong, X., Castarède, D., Boucly, A., Artiglia, L., Ammann, M., Bartels-Rausch, T., Thomson, E. S., and Pettersson, J. B. C.: Reversibly physisorbed and chemisorbed water on carboxylic salt surfaces under atmospheric conditions, J. Phys. Chem. C, 124, 5263–5269, https://doi.org/10.1021/acs.jpcc.0c00319, 2020.

Koop, T. and Zobrist, B.: Parameterizations for ice nucleation in biological and atmospheric systems, Phys. Chem. Chem. Phys., 11, 10839–10850, https://doi.org/10.1039/B914289D, 2009.

Koop, T., Kapilashrami, A., Molina, L. T., and Molina, M. J.: Phase transitions of sea-salt/water mixtures at low temperatures: Implications for ozone chemistry in the polar marine boundary layer, J. Geophys. Res.-Atmospheres, 105, 26393–26402, https://doi.org/10.1029/2000jd900413, 2000.

Křepelová, A., Huthwelker, T., Bluhm, H., and Ammann, M.: Surface chemical properties of eutectic and frozen NaCl solutions probed by XPS and NEXAFS, ChemPhysChem, 11, 3859–3866, https://doi.org/10.1002/cphc.201000461, 2010a.

Křepelová, A., Newberg, J., Huthwelker, T., Bluhm, H., and Ammann, M.: The nature of nitrate at the ice surface studied by XPS and NEXAFS, Phys. Chem. Chem. Phys., 12, 8870–8880, https://doi.org/10.1039/C0CP00359J, 2010b.

Kuhn, J., Stutz, J., Bartels-Rausch, T., Thomas, J. L., Cesler-Maloney, M., Simpson, W. R., Dibb, J. E., Heinlein, L. M. D., and Anastasio, C.: The interplay between snow and polluted air masses in cold urban environments, Faraday Discuss., 258, 502–520, https://doi.org/10.1039/D4FD00176A, 2025.

Li, X., Ye, C., Lu, K., Xue, C., Li, X., and Zhang, Y.: Accurately predicting spatiotemporal variations of near-surface nitrous acid (HONO) based on a deep learning approach, Environ. Sci. Technol., 58, 13035–13046, https://doi.org/10.1021/acs.est.4c02221, 2024.

Marrocco, H. A. and Michelsen, R. R. H.: Nitrate concentration near the surface of frozen aqueous solutions, J. Phys. Chem. B, 118, 14929–14941, https://doi.org/10.1021/jp508244u, 2014.

https://doi.org/10.5194/egusphere-2026-3716
Preprint. Discussion started: 27 July 2026


Marti, J. and Mauersberger, K.: A survey and new measurements of ice vapor pressure at temperatures between 170 and 250 K, Geophys. Res. Lett., 20, 363–366, https://doi.org/10.1029/93GL00105, 1993.

McFall, A. S., Edwards, K. C., and Anastasio, C.: Nitrate photochemistry at the air–ice interface and in other ice reservoirs, Environ. Sci. Technol., 52, 5710–5717, https://doi.org/10.1021/acs.est.8b00095, 2018a.

McFall, A. S., Edwards, K. C., and Anastasio, C.: Nitrate Photochemistry at the Air–Ice Interface and in Other Ice Reservoirs, Environ. Sci. Technol., 52, 5710–5717, https://doi.org/10.1021/acs.est.8b00095, 2018b.

Morenz, K. J. and Donaldson, D. J.: Chemical morphology of frozen mixed nitrate–salt solutions, J. Phys. Chem. A, 121, 2166–2171, https://doi.org/10.1021/acs.jpca.6b12608, 2017.

Morenz, K. J., Shi, Q., Murphy, J. G., and Donaldson, D. J.: Nitrate photolysis in salty snow, J. Phys. Chem. A, 120, 7902–7908, https://doi.org/10.1021/acs.jpca.6b06685, 2016.

Murata, T., Matsukawa, T., and Naoé, S.: Na K-XANES and EXAFS studies in sodium halides, Phys. B Condens. Matter, 158, 610–612, https://doi.org/10.1016/0921-4526(89)90407-9, 1989a.

Murata, T., Matsukawa, T., and Naoé, S.: Na K-XANES and EXAFS studies in sodium halides, Phys. B Condens. Matter, 158, 610–612, https://doi.org/10.1016/0921-4526(89)90407-9, 1989b.

Murphy, D. M. and Koop, T.: Review of the vapour pressures of ice and supercooled water for atmospheric applications, Q. J. R. Meteorol. Soc., 131, 1539–1565, https://doi.org/10.1256/qj.04.94, 2005.

Orlando, F., Waldner, A., Bartels-Rausch, T., Birrer, M., Kato, S., Lee, M.-T., Proff, C., Huthwelker, T., Kleibert, A., van Bokhoven, J., and Ammann, M.: The Environmental Photochemistry of Oxide Surfaces and the Nature of Frozen Salt Solutions: A New in Situ XPS Approach, Top. Catal., 59, 591–604, https://doi.org/10.1007/s11244-015-0515-5, 2016.

Prado, R. J. and Flank, A. M.: Sodium K-edge XANES calculation in “NaCl” type structures, Phys. Scr., 2005, 165, https://doi.org/10.1238/Physica.Topical.115a00165, 2005.

Preobrajenski, A. B., Vinogradov, A. S., Molodtsov, S. L., Krasnikov, S. K., Chassé, T., Szargan, R., and Laubschat, C.: Molecular effects in solid $NaNO_3$ observed by x-ray absorption and resonant Auger spectroscopy, Phys. Rev. B, 65, 205116, https://doi.org/10.1103/PhysRevB.65.205116, 2002.

Preobrajenski, A. B., Vinogradov, A. S., Krasnikov, S. A., Szargan, R., and Mårtensson, N.: Molecular nature of resonant X-ray scattering in solid $LiNO_3$, Phys. Rev. B, 69, 115116, https://doi.org/10.1103/PhysRevB.69.115116, 2004.

Rekhtina, M., Bugaev, A., Dunstan, M. T., Dal Pozzo, A., Nadjafi, M., Borca, C., Huthwelker, T., Abdala, P. M., and Müller, C. R.: Probing the local structure of Na in $NaNO_3^-$ promoted, MgO-based $CO_2$ sorbents via X-ray absorption spectroscopy, Chem. Mater., 35, 10060–10069, https://doi.org/10.1021/acs.chemmater.3c02077, 2023.

Rowlinson, M. J., Carpenter, L. J., Evans, M. J., Lee, J. D., Andersen, S. T., Sherwen, T., Callaghan, A. B., Sommariva, R., Bloss, W., Hou, S., Crilley, L. R., Pfeilsticker, K., Weyland, B., Ryerson, T. B., Veres, P. R., Campuzano-Jost, P., Guo, H., Nault, B. A., Jimenez, J. L., and Fomba, K. W.: A nitrate photolysis source of tropospheric HONO is incompatible with current understanding of atmospheric chemistry, Atmospheric Chem. Phys., 25, 16945–16968, https://doi.org/10.5194/acp-25-16945-2025, 2025.

Ruiz-Lopez, M. F., Francisco, J. S., Martins-Costa, M. T. C., and Anglada, J. M.: Molecular reactions at aqueous interfaces, Nat. Rev. Chem., 4, 459–475, https://doi.org/10.1038/s41570-020-0203-2, 2020.

https://doi.org/10.5194/egusphere-2026-3716
Preprint. Discussion started: 27 July 2026


Shah, V., Jacob, D. J., Dang, R., Lamsal, L. N., Strode, S. A., Steenrod, S. D., Boersma, K. F., Eastham, S. D., Fritz, T. M., Thompson, C., Peischl, J., Bourgeois, I., Pollack, I. B., Nault, B. A., Cohen, R. C., Campuzano-Jost, P., Jimenez, J. L., Andersen, S. T., Carpenter, L. J., Sherwen, T., and Evans, M. J.: Nitrogen oxides in the free troposphere: Implications for tropospheric oxidants and the interpretation of satellite $NO_2$ measurements, Atmos Chem Phys, 23, 1227–1257, https://doi.org/10.5194/acp-23-1227-2023, 2023.

Shi, Q., Tao, Y., Krechmer, J. E., Heald, C. L., Murphy, J. G., Kroll, J. H., and Ye, Q.: Laboratory investigation of renoxification from the photolysis of inorganic particulate nitrate, Environ. Sci. Technol., 55, 854–861, https://doi.org/10.1021/acs.est.0c06049, 2021.

Smith, J. W., Lam, R. K., Shih, O., Rizzuto, A. M., Prendergast, D., and Saykally, R. J.: Properties of aqueous nitrate and nitrite from x-ray absorption spectroscopy, J. Chem. Phys., 143, https://doi.org/10.1063/1.4928867, 2015.

Takenaka, N., Ueda, A., and Maeda, Y.: Acceleration of the rate of nitrite oxidation by freezing in aqueous solution, Nature, 358, 736–738, https://doi.org/10.1038/358736a0, 1992.

Tang, I. N. and Munkelwitz, H. R.: Composition and temperature dependence of the deliquescence properties of hygroscopic aerosols, Atmospheric Environ. Part Gen. Top., 27, 467–473, https://doi.org/10.1016/0960-1686(93)90204-C, 1993.

Van der Ham, F., Witkamp, G. J., De Graauw, J., and Van Rosmalen, G. M.: Eutectic freeze crystallization: Application to process streams and waste water purification, Chem. Eng. Process. Process Intensif., 37, 207–213, https://doi.org/10.1016/S0255-2701(97)00055-X, 1998.

Warneck, P. and Wurzinger, C.: Product quantum yields for the 305-nm photodecomposition of nitrate in aqueous solution, J. Phys. Chem., 92, 6278–6283, https://doi.org/10.1021/j100333a022, 1988.

Wren, S. N., Donaldson, D. J., and Abbatt, J. P. D.: Photochemical chlorine and bromine activation from artificial saline snow, Atmospheric Chem. Phys., 13, 9789–9800, https://doi.org/10.5194/acp-13-9789-2013, 2013.

Yasuda, I., Endo, K., Arai, N., and Yasuoka, K.: In-layer inhomogeneity of molecular dynamics in quasi-liquid layers of ice, Commun. Chem., 7, 117, https://doi.org/10.1038/s42004-024-01197-0, 2024.

Yoshimura, T., Tamenori, Y., Suzuki, A., Kawahata, H., Iwasaki, N., Hasegawa, H., Nguyen, L. T., Kuroyanagi, A., Yamazaki, T., Kuroda, J., and Ohkouchi, N.: Altervalent substitution of sodium for calcium in biogenic calcite and aragonite, Geochim. Cosmochim. Acta, 202, 21–38, https://doi.org/https://doi.org/10.1016/j.gca.2016.12.003, 2017.